Composite particle production in relativistic Au+Pt, Si+Pt, and p+Pt collisions

N. Saito,[5] B. Bassalleck,[7] T. Bürger,[4] M. Burger,[4] R. Chrien,[2] G. E. Diebold,[9]
H. En'yo,[5] G. Franklin,[3]
J. Franz,[4] T. Iijima,[5] K. Imai,[5] J. Lowe,[7,1] R. Magahiz,[3] A. Masaike,[5]
F. Merrill,[3] J. M. Nelson,[1]
K. Okada,[6] P. Pile,[2] B. Quinn,[3] E. Rössle,[4] A. Rusek,[7] R. Sawafta,[2]
H. Schmitt,[4] R. A. Schumacher,[3]
R. L. Stearns,[8] R. Sukaton,[3] R. Sutter,[2] F. Takeutchi,[6] D. M. Wolfe,[7]
S. Yokkaichi,[5] V. Zeps,[3] and R. Zybert[1]
(E886 Collaboration)

[1]*Department of Physics, University of Birmingham, Birmingham B15 2TT, United Kingdom*
[2]*Brookhaven National Laboratory, Upton, New York 11973*
[3]*Department of Physics, Carnegie Mellon University, Pittsburgh, Pennsylvania 15213*
[4]*Fakultaet f. Physik, University of Freiburg, D-79104 Freiburg, Germany*
[5]*Department of Physics, Kyoto University, Kyoto 606, Japan*
[6]*Faculty of Science, Kyoto Sangyo University, Kyoto 603, Japan*
[7]*Department of Physics, University of New Mexico, Albuquerque, New Mexico 87131*
[8]*Department of Physics and Astronomy, Vassar College, Poughkeepsie, New York 12601*
[9]*Physics Department, Yale University, New Haven, Connecticut 06511*

(Received 11 January 1994)

Recently, highly relativistic Au beams have become available at the Brookhaven National Laboratory Alternating Gradient Synchrotron. Inclusive production cross sections for composite particles, d, t, ^{3}He, and ^{4}He, in 11.5A GeV/c Au+Pt collisions have been measured using a beam line spectrometer. For comparison, composite particle production was also measured in Si + Pt and p + Pt collisions at similar beam momenta per nucleon (14.6A GeV/c and 12.9 GeV/c, respectively). The projectile dependence of the production cross section for each composite particle has been fitted to $A_{\rm proj}^{\alpha}$. The parameter α can be described by a single function of the mass number and the momentum per nucleon of the produced particle. Additionally, the data are well described by momentum-space coalescence. Comparisons with similar analysis of Bevalac A + A data are made. The coalescence radii extracted from momentum-space coalescence fits are used to determine reaction volumes ("source size") within the context of the Sato-Yazaki model.

PACS number(s): 25.75.+r

I. INTRODUCTION

The size of interaction volume, or "source size," is one of the most basic characteristics of the highly excited hadronic state produced in heavy ion collisions. Extensive efforts have been made to determine the source sizes in A + A collisions over a wide range of nuclei and momenta. These efforts commonly examine multiparticle correlations such as pion interferometry [1]. Along the same lines, light nuclei synthesized in the reaction volume are further examples of highly correlated multiparticle final states produced in the collisions. As such, the yields of these composite object may provide a (semi)quantitative measure of the reaction source size in these collisions. In this pursuit, various coalescence models have been developed [2–5].

Empirically, the production of mass A nuclei in nucleus-nucleus collisions has been observed to scale as the Ath power of the observed nucleon spectra [6–12]. Such behavior could result from a coalescence production mechanism whereby nucleons sufficiently close together in phase space would bind to form light nuclei. The probability of forming such clusters depends strongly on the density and distribution of the nucleon constituents in the hadronic system formed in the collision. As a result, the observed yields of light nuclei will depend on the reaction source size and can be used to measure this characteristic of the system.

Mekjian [2] and Sato and Yazaki [3] have developed coalescence models from which a reaction source size may be deduced. These models were originally developed within the context of light-nucleus production in low-energy A + A collisions. However, with the initiation of the relativistic heavy ion programs at the Brookhaven National Laboratory (BNL) Alternating Gradient Synchrotron (AGS) and at the European Organization for Nuclear Research Super Proton Synchrotron, such studies of light composite object production in A + A collisions are now being extended to higher energies [13–15]. In particular, the recent acceleration of Au ions at the AGS has provided an opportunity to extend coalescence studies to very large relativistic systems. Taking advantage of this opportunity, we have measured inclusive production cross sections for p, d, t, ^{3}He, and ^{4}He in

11.5A GeV/c Au + Pt collisions. For comparison, the cross sections have also been measured in Si + Pt collisions at 14.6A GeV/c and in p + Pt collisions at 12.9 GeV/c. The Au + Pt and Si + Pt reactions were studied at the BNL AGS while the p + Pt reaction was studied at the National Laboratory for High Energy Physics (KEK) using the Proton Synchrotron (PS) there.

Each of these measurements was made using a secondary beam line as a mass spectrometer. This approach greatly simplifies particle identification under the high multiplicity conditions of heavy ion collisions. The disadvantage of this technique is that the kinematical region of the measurement is limited.

The outline of this paper is as follows. Following the description of the experimental apparatus in Sec. II, the measured cross sections are presented in Sec. III. In Sec. IV, the discussion is focused on the applicability of the coalescence model to our data and the determination of the source size with the Sato-Yazaki model. A comparison with Bevalac data is made. The validity of the coalescence picture will be discussed in Sec. V.

II. EXPERIMENTAL METHOD

As mentioned above, this paper is based on two experiments. For each reaction, a thin Pt target of approximately 6–7 % of an interaction length (1.5 mm, 2.8 mm, and 5.0 mm for the Au + Pt, Si + Pt, and p + Pt reactions, respectively) was used together with a beam line spectrometer system. The Au + Pt and Si + Pt reactions were studied at the AGS using the D6 secondary beam line [16] and the associated dipole spectrometer constructed for the AGS experiment 813/836 H particle search [17]. The p + Pt reaction was studied at the KEK PS using the T3 beam line spectrometer. A schematic layout of the D6 beam line spectrometer is shown in Fig. 1(a) while that of the T3 beam line spectrometer is shown in Fig. 1(b). The characteristics of each beam line are summarized in Table I. The beam line phase space acceptances were calculated using the Monte Carlo simulation program DECAY TURTLE [18].

Measurements of p, d, t, ^{3}He, and ^{4}He cross sections were made for magnetic rigidities of p/Z =0.8, 1.2, 1.5, and 1.8 GeV/c for the Au + Pt reaction. Measurements were made at a rigidity of 1.8 GeV/c for the Si + Pt reaction and at 1.2, 1.5, and 1.8 GeV/c for the p + Pt reaction. In addition to the measurements of composite particle production reported here, cross sections for $\pi^{\pm}$, $K^{\pm}$, and $\bar{p}$ were measured and are reported elsewhere [19].

TABLE I. The characteristics of the D6 and the T3 beam lines.

	D6 line, BNL AGS	T3 line, KEK PS
Production angle	5.7°	5.7°
$\Delta p/p$	±2.1%	±0.8%
Horizontal acceptance	± 30 mrad	± 3.1 mrad
Vertical acceptance	± 4.6 mrad	± 8.9 mrad
$\Delta p \Delta\Omega/p$	11.1 msr %	0.45 msr %

The beam intensity during the Si run was often as high as 10^9 ions per spill (spill length $\approx$ 1 s) while the intensity reached 10^7 ions per spill during the Au run. To monitor the beam intensity on target, the integrated charge from two ionization chambers was used. The first chamber was placed in the primary beam (in-beam chamber) and monitored the total beam delivered to the target area. This chamber was calibrated in place using a plastic scintillation counter during periods of low beam intensity ($\sim$ 5×10^5 per spill). The second chamber was placed out of beam near the production target (out-of-beam chamber) and monitored the average flux of produced particles. The ratio of integrated charge from these chambers provided a relative measure of incident beam on target. This ratio was used to correct for variations throughout the runs due primarily to horizontal instability (i.e., "sweeping") of the beam spot on the target.

In the case of the proton beam at KEK, the beam intensity was typically 10^{11} protons per spill (spill length $\approx$ 2.0 s). The primary beam flux was monitored with a secondary emission chamber placed in front of the Pt target. The chamber was calibrated by activation immediately following the p + Pt measurements. Targeting conditions were monitored using a plastic scintillation telescope consisting of three in-line counters looking at the target. This device monitored the flux of particles produced at the target. As in the case of Au and Si runs, the ratio of the counts from these detectors provided the relative targeting efficiency throughout the run.

In each reaction, particles were selected by a delayed coincidence between two scintillation counters placed in the beam line. For the Au and Si runs, one counter

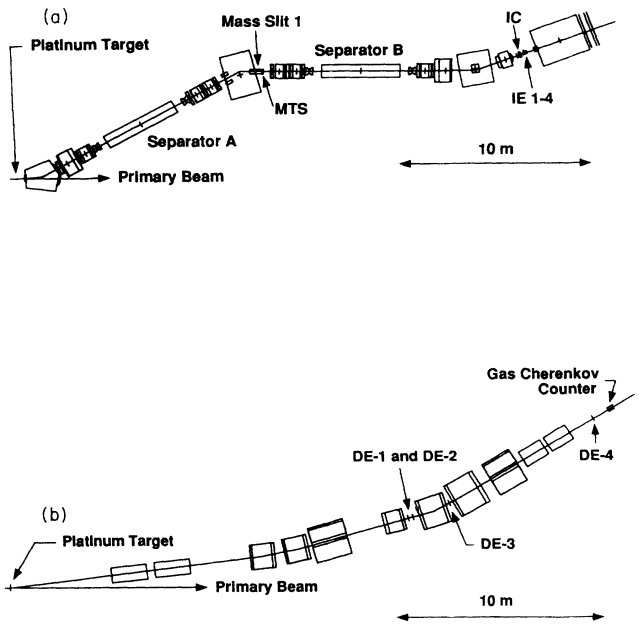

FIG. 1. Schematic views of (a) the D6 beam line (BNL AGS) and E886 apparatus and (b) the T3 beam line (KEK PS) and relevant experimental apparatus.

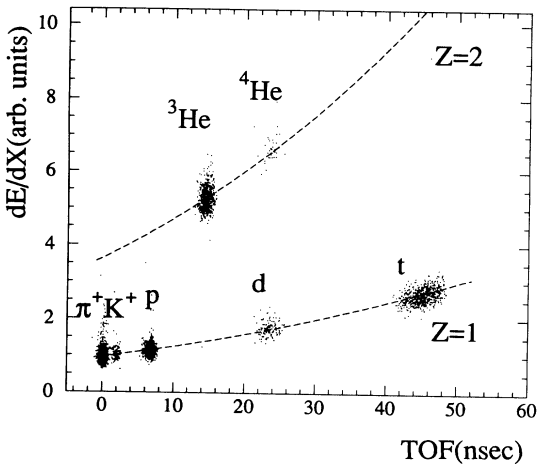

FIG. 2. Time of flight spectra for positive particles produced with a rigidity of 1.8 GeV/c in Au + Pt collisions at 11.5A GeV/c. Plotted is the energy loss (dE/dX) versus time of flight relative to a speed of light particle.

(MTS) was located just downstream of the first mass slit while the other (IE-1) was placed at the final focus of the beam line. The distance between these two counters was about 15.1 m. For the p + Pt measurements, the DE-1 and DE-4 counters were used [Fig. 1(b)]; these were separated by a flight path of 11.5 m. Several triggers spanning different time-of-flight (TOF) ranges were used with appropriate prescale factors to enhance the selection of rare nuclear species written to tape.

Particle identification was made using the TOF and energy loss dE/dX recorded by the in-beam scintillation counters. The energy loss was determined by taking a truncated mean of pulse heights. For this an average of the two lowest pulse heights in the IE or DE counters was used to reduce the Landau tail of energy deposits in the scintillators. A two-dimensional histogram of dE/dX versus TOF obtained for an Au run at +1.8 GeV/c is shown in Fig. 2. Here the π^+, K^+, p, and d abundances were suppressed by a prescale factor of 100. As is readily apparent in this figure, particles could be identified with almost no background.

III. CROSS SECTIONS FOR COMPOSITE PARTICLE PRODUCTION

The invariant differential cross sections $E\frac{d^3\sigma}{dp^3}$ for inclusive p, d, t, ^{3}He, and ^{4}He production are listed in Table II for each reaction. Statistical errors are indicated as well.

Relative systematic uncertainties mainly came from the acceptance calculation and are estimated to be 15%, 5%, and 10% for the Au + Pt, Si + Pt, and p + Pt reactions, respectively. Overall systematic uncertainties are originated in the flux monitor calibration and the target thickness. They are estimated to be 16%, 11%, and 11% for the Au, Si, and p induced reactions, respectively. As a result of erratic targeting conditions during the Au beam run, the reliability of the cross section normalization is

TABLE II. The invariant cross sections of particle production at 5.7° (laboratory angle) in p + Pt, Si + Pt, and Au + Pt, collisions at 12.9 GeV/c, 14.6A GeV/c, and 11.5A GeV/c, respectively. Only statistical errors are indicated here. Unless specified, statistical errors are less than 3%. Overall systematic uncertainties are estimated to be 11%, 11%, and 16% for the p + Pt, Si + Pt, and Au + Pt reactions, respectively, while relative uncertainties are estimated to be 10%, 5%, and 15%, respectively.

Particle	p/Z (GeV/c)	p + Pt (mb/GeV^2)	Si + Pt (mb/GeV^2)	Au + Pt (mb/GeV^2)
p	1.8	5.61×10^2	8.16×10^3	6.67×10^4
	1.5	7.47×10^2		6.24×10^4
	1.2	1.13×10^3		7.29×10^4
	0.8			9.37×10^4
d	1.8	4.13×10^1	$6.91(0.27) \times 10^2$	$3.24(0.12) \times 10^3$
	1.5	8.54×10^1		$3.46(0.16) \times 10^3$
	1.2	1.90×10^2		$6.75(0.36) \times 10^3$
	0.8			$1.12(0.07) \times 10^4$
t	1.8	6.46×10^0	$8.50(1.07) \times 10^1$	$3.86(0.45) \times 10^2$
	1.5	1.58×10^1		$4.86(0.71) \times 10^2$
	1.2			$9.86(1.64) \times 10^2$
	0.8			
^{3}He	1.8	1.06×10^{-1}	$6.70(1.24) \times 10^0$	$3.53(0.57) \times 10^1$
	1.5	3.07×10^{-1}		$5.94(0.99) \times 10^1$
	1.2	$8.64(0.63) \times 10^{-1}$		$9.61(1.96) \times 10^1$
	0.8			$2.08(0.39) \times 10^2$
^{4}He	1.8	$1.02(0.07) \times 10^{-2}$	$7.87(4.54) \times 10^{-1}$	$3.07(0.76) \times 10^0$
	1.5	$4.46(0.22) \times 10^{-2}$		$5.35(1.33) \times 10^0$
	1.2	$2.10(0.38) \times 10^{-1}$		$1.15(0.38) \times 10^1$
	0.8			$3.98(1.99) \times 10^1$

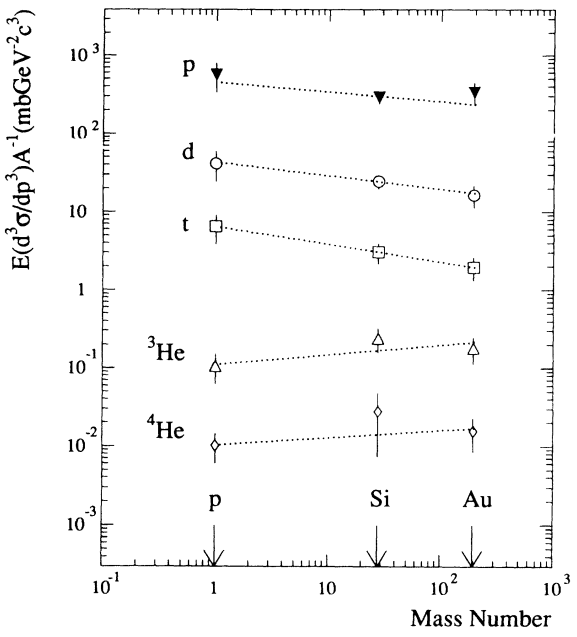

FIG. 3. Projectile mass dependence of the 5.7° invariant cross sections at rigidity p/Z=1.8 GeV/c. The dotted lines are the results of fits to $A^{\alpha}_{\rm proj}$.

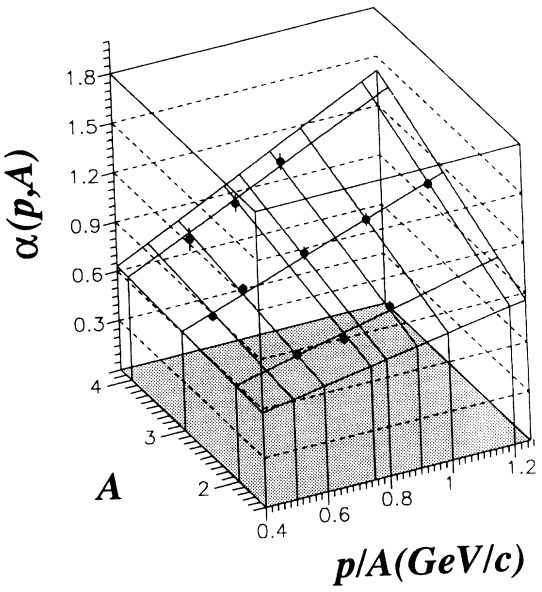

FIG. 4. Projectile mass dependence parameter α plotted as a function of the momentum per nucleon P/A and mass number A. Clearly α increases with mass number and momentum per nucleon. The grid represents the result of a fit to the functional form: $\alpha(p,A) = (\xi p + \eta)A + \zeta$ (see text for details).

reduced. Consequently, relative and overall uncertainties for measurements with the Au beam are somewhat larger than for those with the Si or proton beams.

To illustrate the projectile mass dependence of the particle yields, Fig. 3 shows the light nucleus production cross sections measured at a rigidity of 1.8 GeV/c. The cross sections shown have been divided by the corresponding mass number of the projectile for each reaction. The dotted lines are the results of the fits assuming the cross sections are proportional to $A^{\alpha}_{\rm proj}$. As seen in this figure, the parameter α is dependent on the produced particle species. To clarify the origin of this dependence, values for α were also determined from the 1.5 GeV/c and 1.2 GeV/c Au + Pt and p + Pt data. Values for α are tabulated in Table III together with the mass number and momentum per nucleon of the produced particle. The dependence of α on mass number and momentum per nucleon ($p = P/A$) is illustrated graphically in Fig. 4. The grid drawn shows the result of a fit for α by the form

$$\alpha(p,A) = (\xi p + \eta)A + \zeta, \tag{1}$$

resulting in $\xi = 0.22 \pm 0.02$, $\eta = -0.07 \pm 0.02$, and $\zeta = 0.55 \pm 0.04$. The reduced χ^2 of the fit was 0.68. As can be seen in Fig. 4, α increases with mass number and momentum per nucleon of the produced particle and is found to exceed unity for the highest masses and momentum per nucleon measured. This behavior suggests collective effects play an important role in the production of composite particles especially for the more massive composites at high momentum per nucleon (i.e., rapidity).

IV. COALESCENCE MODEL ANALYSIS

Previous measurements of light-nucleus production have been well described by coalescence models [6–12]. Empirically it was noted that the production cross section of light nuclei with Z protons and N neutrons could

TABLE III. Projectile mass dependence parameter α for various composite species and rigidities. At 1.8 GeV/c the composite spectra from all three reactions were fit to the form $A^{\alpha}_{\rm proj}$. At 1.5 and 1.2 GeV/c, α was determined using the Au + Pt and p + Pt measurements only. Consequently, no χ^2 fit was required.

		p (A = 1)	d (A = 2)	t (A = 3)	^{3}He (A = 3)	^{4}He (A = 4)
1.8 GeV/c	α	0.88±0.03	0.83±0.03	0.77±0.03	1.12±0.03	1.09±0.05
	χ^2	19.8	0.63	0.00[a]	5.08	1.55
1.5 GeV/c	α	0.84±0.03	0.70±0.03	0.65±0.03	1.00±0.04	0.91±0.05
1.2 GeV/c	α	0.79±0.03	0.68±0.03		0.89±0.04	0.76±0.07

[a]The χ^2 value is accidentally very small, 3.32×10^{-4}.

be related to the observed proton spectra according to

$$E_A \frac{d^3\sigma_A(P_A)}{dP_A^3} = C_A \left(E_p \frac{d^3\sigma_p}{dp_p^3} \right)^A . \quad (2)$$

Here σ_A stands for the production cross section of a composite particle of mass number A, P_A is the momentum of the composite particle, σ_p is the production cross section of protons, and C_A is a proportionality constant which depends upon the produced nuclear species and the production reaction being studied. The proton momentum p_p is equal to the momentum per nucleon of the produced composite particle p $(=P_A/A)$.

It was quickly noted that such power law scaling of the invariant proton cross section is consistent with a momentum space overlap of coalescing nucleons. In the simplest picture, nucleons may coalesce to form light nuclei if the momentum difference between the constituent nucleons is less than some cutoff value $\tilde{p_0}$. In this case, the proportionality constant C_A can be related to the cutoff $\tilde{p_0}$ according to [8]

$$C_A = \frac{2s+1}{2^A} \frac{1}{N!Z!} \left(\frac{N_{\rm proj} + N_{\rm targ}}{Z_{\rm proj} + Z_{\rm targ}} \right)^N \times A \left(\frac{1}{m\sigma_0} \frac{4\pi\tilde{p_0}^3}{3} \right)^{A-1} . \quad (3)$$

Here $A = Z + N$, s is the spin of the produced nucleus, $N_{\rm targ}$ $(N_{\rm proj})$ and $Z_{\rm targ}$ $(Z_{\rm proj})$ are the neutron and proton number of the target (projectile) nuclei, m is the nucleon mass, σ_0 is usually taken as the nucleus-nucleus inelastic cross section, and $\tilde{p_0}$ is commonly referred to as the coalescence radius.

The values of σ_0 were estimated by simulation using a Woods-Saxon distribution to describe the nuclear density of the colliding A + Pt system. Interacting nucleons were defined as constituents which pass within a distance $\sqrt{\sigma_{NN}/\pi}$ of each other, where σ_{NN} is the total N + N cross section (= 40 mb). The simulation reproduces measured inelastic cross sections for various colliding systems [19].

To examine the present light-nucleus cross sections in this framework, the momentum dependence of the proton spectra was assumed to be representable as a sum of two exponentials:

$$E_p \frac{d^3\sigma_p}{dp_p^3} = \exp(\alpha_1 + \beta_1 p) + \exp(\alpha_2 + \beta_2 p). \quad (4)$$

Using this shape function, the measured proton and light-nucleus cross sections were simultaneously fit to Eq. (2). The results of the best fit are summarized in Table IV. These are shown in Fig. 5(a) for the Au + Pt data and Fig. 5(b) for the p + Pt data along with the measured cross sections. As can be seen, the model reproduces the composite particle spectra well in each case.

A comparison of the coalescence factors determined in these fits with those from measurements at the Bevalac $(E/A \leq 2.1$ GeV) [9, 10] is shown in Fig. 6. Plotted is

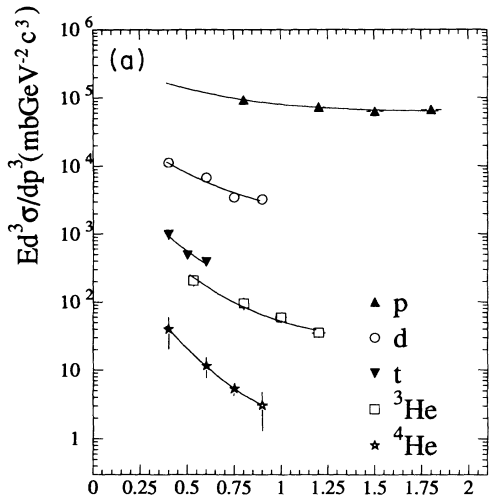

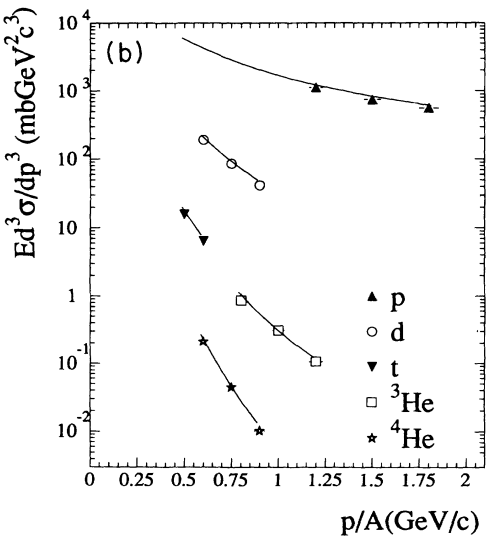

FIG. 5. Cross sections of light-nucleus production at 5.7° in (a) Au + Pt collisions and (b) p + Pt collisions are shown as a function of the momentum per nucleon P/A of a produced particle. The lines are the results of a coalescence fit (see text for details).

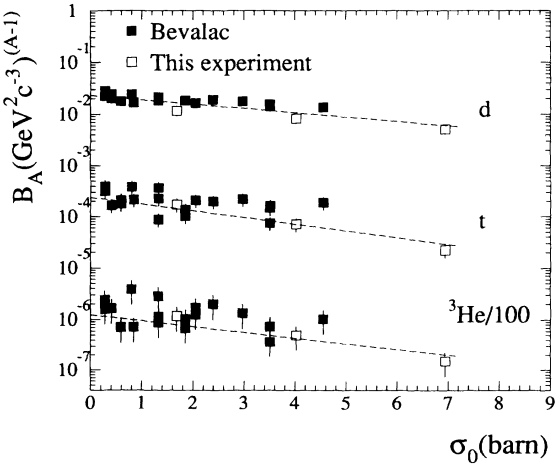

FIG. 6. Coalescence factors B_A for various reactions are plotted versus σ_0 without regard to incident projectile energy. Dashed lines show the results of the fit to all data assuming $B_A = \exp(\xi + \eta\sigma_0)$.

TABLE IV. Results of coalescence model fits of the composite particle production cross sections by Eq. (2). A functional form of proton momentum spectrum was empirically assumed as a sum of two exponentials. C_A is a coalescence probability, $\tilde{p_0}$ is a coalescence radius, $R_{\rm SY}$ is a source size deduced from coalescence radius with the Sato-Yazaki model, and $R_{\rm PIS}$ is a source size deduced assuming that the source size is independent of the produced particle (see text for details).

	p + Pt	Si + Pt	Au + Pt
σ_0 (mb)	1681	4025	6941
first component	$\exp(10.4 - 4.34p)$	$\exp(10.9 - 2.58p)$	$\exp(12.7 - 2.91p)$
second component	$\exp(8.04 - 0.91p)$	$\exp(10.1 - 0.63p)$	$\exp(11.0 - 0.01p)$
C_d	1.13×10^{-5}	1.92×10^{-6}	4.13×10^{-7}
C_t	9.14×10^{-11}	3.80×10^{-12}	2.12×10^{-13}
$C_{^3\rm He}$	6.42×10^{-11}	2.67×10^{-12}	1.02×10^{-13}
$C_{^4\rm He}$	6.96×10^{-16}	5.34×10^{-18}	5.66×10^{-20}
$\tilde{p_0}(d)$ (MeV/c)	124±9	93.3±4.5	65.9±1.9
$\tilde{p_0}(t)$ (MeV/c)	158±9	126±8	92.0±2.2
$\tilde{p_0}(^3\rm He)$ (MeV/c)	159±7	126±8	87.2±1.9
$\tilde{p_0}(^4\rm He)$ (MeV/c)	186±9	146±10	105±3
$R^d_{\rm SY}$ (fm)	1.28±0.54		5.00±0.19
$R^t_{\rm SY}$ (fm)	2.01±0.24		4.48±0.13
$R^{^3\rm He}_{\rm SY}$ (fm)	1.98±0.18		4.78±0.12
$R^{^4\rm He}_{\rm SY}$ (fm)	2.09±0.16		4.41±0.12
$R^{\rm av}_{\rm SY}$ (fm)	1.81±0.33		4.67±0.23
$\chi^2_{\rm SY}/N_{\rm d.f.}$	1.02/5		8.44/11
$R_{\rm PIS}$ (fm)	2.28±0.12	2.95±0.26	4.27±0.14
$\chi^2_{\rm PIS}/N_{\rm d.f.}$	6.24/8	0/0	22.8/14

the quantity B_A ($= C_A\sigma_0^{A-1}$) versus σ_0. As can be seen from Eq. (3), the quantity B_A depends mostly on the coalescence radius $\tilde{p_0}$. The present results for the t and ^{3}He yields in p + Pt and Si + Pt are not significantly different from the Bevalac data despite approximately an order of magnitude difference in beam energy per nucleon. However, the present d coalescence probabilities consistently fall below the lower-energy data by about a factor of 0.5 – 0.7. For all particles, the coalescence factors show a clear dependence on σ_0 which seems to be roughly the same for both the present results and the Bevalac data. Since the reaction cross section σ_0 is largely a consequence of the size of the colliding nuclei, this behavior empirically demonstrates an underlying relationship between the coalescence probability and the size of the colliding system.

Several authors have attempted to quantify this relationship in order to extract a reaction source size based on the measured coalescence probabilities. In this paper we will apply the model of Sato and Yazaki [3] to arrive at a semiquantitative measure of source sizes for the p + Pt, Si + Pt, and Au + Pt reactions studied.

According to the Sato-Yazaki model, the coalescence radius empirically determined from Eqs. (2) and (3) can be related to the source size as

$$p_0 = \frac{\kappa\hbar}{\sqrt{R^2_{\rm SY} + R^2_c}}, \tag{5}$$

where

$$(p_0^3)^{A-1} = A^3\frac{2s+1}{2^A}(\tilde{p_0^3})^{A-1}. \tag{6}$$

Here κ is a phase space factor which is determined by the mass number and spin of produced particles, R_c is the root mean square radius of the wave function of the produced particle, and $R_{\rm SY}$ is the rms radius of the source. The wave function of produced nuclei and the spatial distribution of nucleons in the highly excited system formed in the collisions (HX) are assumed to be spherically symmetric Gaussian distributions. Values for κ are 3.46, 3.16, 3.16, and 2.91 for d, t, ^{3}He, and ^{4}He, respectively, and the R_c values are 2.739, 2.041, 2.041, and 1.608 fm for d, t, ^{3}He, and ^{4}He, respectively. These values are taken from Refs. [3, 20]. The source sizes obtained are listed in Table IV for the p + Pt and Au + Pt data.

In light of the limited (i.e., single rigidity) measurements made for the Si + Pt reaction, a slightly different approach was adopted to determine source size from the measured light-nucleus yields. As shown for the p + Pt and Au + Pt reactions in Table IV, the particle dependence of the source size deduced with the Sato-Yazaki model is rather weak. Exploiting this, we made the simplifying assumption of particle independent source size to analyze the Si + Pt reaction, namely, $R^d_{\rm SY}$=$R^t_{\rm SY}$=$R^{^3\rm He}_{\rm SY}$=$R^{^4\rm He}_{\rm SY}$=$R_{\rm PIS}$. This reduces the number of free parameters in the coalescence fit and allows a source size to be determined based solely on the light-nucleus cross sections measured at a fixed rigidity (i.e., at 1.8 GeV/c). A source size of 2.95±0.26 fm is found for the Si + Pt reaction and is listed in Table IV. As one might expect, this value is considerably smaller ($\approx$ 30%) than that reported by E802/E859 and E814 based on two-proton correlation measurements in *central* Si + Au [14] and Si + Pb [21] collisions.

To compare the source size for each reaction on the same basis, two approaches were taken. One was to compare the averages of particle-dependent source sizes

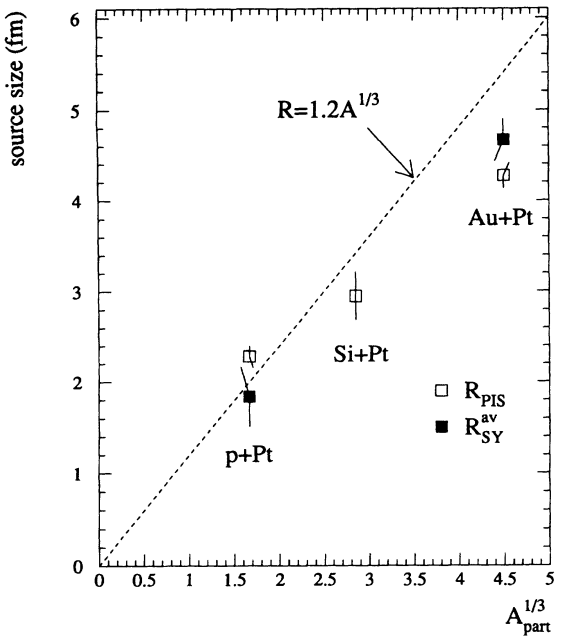

FIG. 7. Source sizes are plotted as a function of the cubic root of the number of participant nucleons $A_{\rm part}$ in collisions. $R^{\rm av}_{\rm SY}$ is the average of the particle dependent source sizes and $R_{\rm PIS}$ is the source size deduced using a particle independent source size constraint. The dashed line indicates normal nuclear density.

($R^{\rm av}_{\rm SY}$) determined above. The other was to fit the p + Pt data and Au + Pt data to Eq. (2) with the particle independent source size constraint ($R_{\rm PIS}$) as was done for the Si + Pt data. These results are also listed in Table IV. Here the error on $R^{\rm av}_{\rm SY}$ is the rms deviations of the particle dependent source sizes.

As seen in Table IV, the source sizes strongly depend on the projectile nucleus. To examine the projectile dependence, we have estimated the average number of participating nucleons in each reaction $A_{\rm part}$ by Monte Carlo simulation. The simulation is basically same as the one used to estimate inelastic cross sections used in the coalescence model analysis. The estimated numbers of participating nucleons $A_{\rm part}$ are 4.66, 23.2, and 91.1 for p + Pt, Si + Pt, and Au + Pt collisions, respectively. The source sizes are plotted as a function of $A^{1/3}_{\rm part}$ in Fig. 7.

For comparison, the dashed line represents normal nuclear density. Some caution is warranted in this comparison since the quantities plotted represent averages over minimum bias collisions and the ratio of two average quantities is not necessarily equal to the average of the corresponding ratio. This caution aside, the relationship between source sizes found with the Sato-Yazaki model and the estimated average number of participants qualitatively suggest a freeze-out density slightly above that of normal nuclear matter. As will be discussed in the following section, source sizes deduced from the Sato-Yazaki model will underestimate the actual source size in the presence of correlations between nucleons in the highly excited system formed in the collision. This would result in an overestimate of the nucleon density at freeze-out.

V. DISCUSSION

As is evident from Fig. 5, the momentum-space coalescence fit is able to describe the present data remarkably well. This raises a question regarding the (presumedly absent) contribution of target fragmentation to the observed composite particle yields. Several remarks on this point are in order. First, the present measurements only extend to momenta per nucleon as low as 0.4 GeV/c or equivalently rapidities as low as $y = 0.4$, still considerably above $y = 0$. Consequently, observed composites resulting from fragmentation would be required to either inherently possess and/or absorb a kick of more than 0.4 GeV/c per nucleon and remain intact. Given a nuclear binding energy of a few MeV per nucleon, it would seem rare indeed for a fragment to absorb such a momentum transfer and not breakup completely.

Second, the question of fragmentation actually points towards a more general question, namely, that of correlations (between nucleons) in the composite particle "source." The observed composite particle spectra (and their relationship to source size) depends upon the degree to which nucleons in the "source" are correlated in position and relative momentum. For example, the Sato-Yazaki calculation of source size assumes position and momenta are distributed independently according to Gaussian distributions. In the presence of a fixed (i.e., rapidity-independent) position-momentum correlation in the source, it is likely that the momentum-space coalescence fit could still provide a good description of the observed composite particle spectra. However, the deduced source size within the context of the Sato-Yazaki model would be incorrect. The question of fragmentation, then, can be expressed in the context of a rapidity-dependent correlation of nucleon position and momentum (e.g., preexisting nucleon clusters in the target nucleus) as well as that of a separate composite particle source, namely, coalescence of cold spectator nucleons. Given the success of the momentum-space coalescence description of the present data, each of these contributions appears relatively small for $y \geq 0.4$. A comparison of the present composite particle yields with those at midrapidity would be particularly interesting and may provide additional insight regarding this question.

As an alternative to the analytical coalescence models applied to the present data, other phenomenological models are being developed within context of various $A + A$ collision simulations (e.g., a relativistic cascade (ARC) and relativistic quantum molecular dynamics (RQMD) [5, 23, 22]). For example, in the work of Ref. [5] using the ARC simulation, nucleons are "coalesced" to form composite particles if they lie within phenomenological cutoffs in position and relative momentum of each other at some point in time following their last interaction. Composite particle measurements, such as the present data set, provide the experimental basis upon which the phenomenological coalescence cutoffs and can be determined. Once these parameters are

fixed, the utility and appeal of such models lies in their ability to predict the abundances of exotic composites such as multistrange hypernuclei ($^{4}_{\Lambda\Lambda}$H,$^{5}_{\Lambda\Lambda}$H, $^{5}_{\Lambda\Lambda}$He,$^{6}_{\Lambda\Lambda}$He, $^{7}_{\Xi^{0}\Lambda\Lambda}$He, etc.). It is possible that such multistrange composites could collapse or decay into stable or metastable configurations (e.g., strangelets). Thus such models can provide a quantitative basis with which null results of strangelet searches in $A + A$ collisions can be examined. Further investigation of composite particle production is warranted in this regard, especially measurements of hypernuclei production in $A + A$ collisions.

VI. CONCLUSION

Cross sections of composite particle production in Au + Pt collision have been measured at several magnetic rigidities. These have been compared with the cross sections in Si + Pt and p + Pt collisions at a similar incident momentum per nucleon. The projectile mass dependence has been fit to $A^{\alpha}_{\rm proj}$ to semiquantitatively compare the three reactions.

Both the data for Au + Pt reaction and the data for p + Pt reaction are shown to be well described within a framework of the coalescence model. The present Si + Pt data are also consistent with this approach. Coalescence probabilities have been compared with those from lower energy measurements performed at the Bevalac. For the most part, the present results are consistent with coalescence probabilities found at lower energies. However, the deuteron coalescence factor appears to fall below that found at lower energies by about a factor of 0.5–0.7.

Source sizes have been determined from the composite particle yields using the Sato-Yazaki model. While the source sizes obtained seem reasonable for each reaction, some caution is warranted since the underlying assumptions of the Sato-Yazaki model may not be valid. Comparison of the source sizes with the estimated number of participating nucleons in each reaction suggest the nucleon density of the systems at freeze-out are similar to that of normal nuclear matter. Further study is required to firmly quantify and refine these techniques for studying the hadronic system formed in $A + A$ collisions.

ACKNOWLEDGMENTS

The authors would like to thank the BNL accelerator and the support staff for their efforts during the runs especially for the successful commissioning of the Au program. Thanks are also given to the members of the PS experiment 257 (APEX) for their willing support during the study of p + Pt reaction at KEK. This work is supported in part by the U.S. Department of Energy under Contracts No. DE-FG02-91ER40609, No. DE-AC02-76H00016, and No. DE-FG04-88ER40396, by German Federal Minister for Research and Technology (BMFT) under Contract No. 06 FR652, by the Japan Society for the Promotion of Science, and by the Monbusho International Scientific Research Program-Joint Research (05044052).

[1] For recent results see R. Albrecht *et al.*, Z. Phys. C **53**, 225 (1992); Nu Xu, in "Proceedings of Heavy Ion Physics at the AGS (HIPAGS '93)," edited by G. S. F. Stephans, S. G. Steadman, and W. L. Kehoe, Massachusetts Institute of Technology Report No. MITLNS-2158, 1993, p. 362 (unpublished).
[2] A. Z. Mekjian, Nucl. Phys. **A312**, 491 (1978).
[3] H. Sato and K. Yazaki, Phys. Lett. **98B**, 153 (1981).
[4] S. Hirenzaki, T. Suzuki, and I. Tanihata, RIKEN, The Institute of Physical and Chemical Research, Report No. RIKEN-AF-NP-141 (unpublished).
[5] C. B. Dover, A. J. Baltz, Y. Pang, T. J. Schlagel, and S. H. Kahana, in "Proceedings of Heavy Ion Physics at the AGS (HIPAGS '93)" [1], p. 213.
[6] V. B. Gavrilov, N. L. Kornienko, G. A. Leskin, and S. V. Semenov, Z. Phys. A **324**, 75 (1986).
[7] K. Nakai, O. Terasaki, T.-A. Shibata, H. En'yo, and I. Arai, Phys. Rev. C **25**, 1992 (1982).
[8] H. H. Gutbrod, A. Sandoval, P. J. Johansen, A. M. Poskanzer, J. Gosset, W. G. Meyer, G. D. Westfall, and R. Stock, Phys. Rev. Lett. **37**, 667 (1976).
[9] M.-C. Lemaire, S. Nagamiya, S. Schnetzer, H. Steiner, and I. Tanihata, Phys. Lett. **85B**, 38 (1979).
[10] S. Nagamiya, M.-C. Lemaire, E. Moeller, S. Schnetzer, G. Shapiro, H. Steiner, and I. Tanihata, Phys. Rev. C **24**, 971 (1981).
[11] K. G. Doss *et al.*, Phys. Rev. C **32**, 116 (1985).
[12] J. F. Amman, P. D. Barnes, M. Doss, S. A. Dytman, R. A. Eisenstein, J. Penkrot, and A. C. Thompson, Phys. Rev. Lett. **35**, 1066 (1975).
[13] J. Barrette *et al.*, Nucl. Phys. **A544**, 432c (1992).
[14] G. S. F. Stephans, in "Proceedings of Heavy Ion Physics at the AGS (HIPAGS '93)" [1], p. 371.
[15] M. Aoki *et al.*, Phys. Rev. Lett. **69**, 2345 (1992).
[16] P. Pile *et al.*, Nucl. Instrum. Methods A **321**, 48 (1992).
[17] P. D. Barnes *et al.*, Nucl. Phys. **A547**, 3c (1992).
[18] K. L. Brown and Ch. Iselin, CERN Report No. 74-2, 1974 (unpublished).
[19] G. E. Diebold *et al.*, Phys. Rev. C **48**, 2984 (1993).
[20] J. C. Bergstrom, Nucl. Phys. **A327**, 458 (1979).
[21] Nu Xu, in "Proceedings of Heavy Ion Physics at the AGS (HIPAGS '93)" [1], p. 362.
[22] H. Sorge, H. Stocker, and W. Greiner, Ann. Phys. (N.Y.) **192**, 266 (1989); Nucl. Phys. **A498**, 567 (1989).
[23] Y. Pang, T. J. Schlagel, and S. H. Kahana, Nucl. Phys. **A544**, 435c (1992).

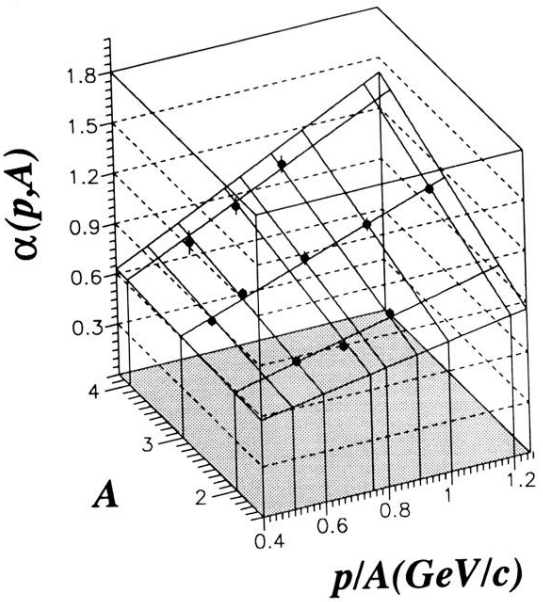

FIG. 4. Projectile mass dependence parameter α plotted as a function of the momentum per nucleon P/A and mass number A. Clearly α increases with mass number and momentum per nucleon. The grid represents the result of a fit to the functional form: $\alpha(p, A) = (\xi p + \eta)A + \zeta$ (see text for details).